Solvation Structure of Hydroxyl Radical by Car−Parrinello Molecular Dynamics

Julia M. Khalack*,†,‡ and Alexander P. Lyubartsev†

Division of Physical Chemistry, Arrhenius Laboratory, Stockholm University, S-106 91 Stockholm, Sweden, and Bogolyubov Institute for Theoretical Physics of the National Academy of Sciences of Ukraine, 14b Metrologichna Str., Kyiv-143, 03143 Ukraine

Received: August 24, 2004; In Final Form: October 22, 2004

Car−Parrinello molecular dynamics simulations of a hydroxyl radical in liquid water have been performed. Structural and dynamical properties of the solvated structure have been studied in details. The partial atom−atom radial distribution functions for the hydrated hydroxyl do not show drastic differences with the radial distribution functions for liquid water. The OH is found to be a more active hydrogen bond donor and acceptor than the water molecule, but the accepted hydrogen bonds are much weaker than for the hydroxide OH^- ion. The first solvation shell of the OH is less structured than the water's one and contains a considerable fraction of water molecules that are not hydrogen bonded to the hydroxyl. Part of them are found to come closer to the solvated radical than the hydrogen bonded molecules do. The lifetime of the hydrogen bonds accepted by the hydroxyl is found to be shorter than the hydrogen bond lifetime in water. A hydrogen transfer between a water molecule and the OH radical has been observed, though it is a much rarer event than a proton transfer between water and an OH^- ion. The velocity autocorrelation power spectrum of the hydroxyl hydrogen shows the properties both of the OH radical in clusters and of the OH^- ion in liquid.

1. Introduction

There exists great interest in the properties of hydroxyl (OH) radical in aqueous media, which arises mostly due to the radical's harmful effects in biological systems.[1−6] The reactions of the OH radical with organic molecules in aqueous solutions can result in abstraction of the H atoms or in its addition to C−C double bonds,[5] which may further lead to destruction of molecular structures. Most of damaging effect of radiation in biological systems comes from the formation of free radicals from the irradiated water and their subsequent interactions with DNA and other biological molecules. Chemical reactions with participation of high concentration OH in the cell cytoplasm have been associated with Parkinson's disease.[7] Hydroxyl radical has been found to be able to induce telomere shortening associated apoptosis in human tumor cells.[8] Properties of OH radical in water are also important in a number of technological applications. For example, in the problem of water purification, the hydroxyl radicals produced by radiolysis of liquid water[2,9] or with the help of heterogeneous photocatalysts[10,11] are widely used.[12−14] In the earth's atmosphere, the OH radicals are dissolved in water droplets, being formed by dissociation of water solvated H_2O_2 or ozone molecules.[15−17] Oxidizing action of the hydrated hydroxyl radical on the soluble organic compounds plays a crucial role in determining their atmospheric lifetimes.[18−23]

Since most of the key hydroxyl reactions occur in aqueous environments, knowledge of the structural and energetic properties of the hydrated radical becomes extremely important. For instance, it has been shown[24] that even a complexation of a hydroxyl radical with a single water molecule may lead to a change of the radical oxidation potential. Also, to consider the oxidation of soluble organic molecules, one needs to know the properties[25] of the fully hydrated radical.[13,26−28] Yet, the solvation structure and dynamics properties of neutral OH in water are virtually unknown. The lifetime of the hydroxyl radical in aqueous environment is of the order of microsecond, which make experimental studies difficult. On the other hand, this lifetime is very long relative to the time scale of molecular motion. That is why theoretical studies, based on ab initio computer simulations may provide valuable information to this problem.

Several ab initio investigations of the OH + H_2O complex in a gas phase[29−33] have been performed. The ground-state geometry with the hydrogen bonding between the water oxygen and the hydroxyl hydrogen was reported. Another configuration, with the hydrogen bonding between the OH oxygen and a water hydrogen, was found to correspond to a local minimum of the potential energy surface. There are also indications[32,34] that a third local minimum geometry is possible with the hydrogen bonding between the hydroxyl oxygen and the both water hydrogens, along with a weak hydrogen bond between the OH hydrogen and the water oxygen.

Other ab initio calculations on the complexes including a hydroxyl radical comprise investigation of the hydrogen bonding between OH and H_2O_2,[35] hydroxyl radical reactions with ketones,[36] polycyclic aromatic hydrocarbons,[37] phenol,[38] dimethyl sulfide,[39] and guanine,[40] cluster model simulation of hydroxyl adsorption on the gold surface,[41] and the production of OH radicals by carbonyl oxides[42] in solution phase. In some works,[42,40] the solvent effects were considered by embedding the studied molecules in a polarizable continuum.

The hydration of the OH radical has been studied by ab initio means for the case of clusters containing up to six water molecules.[34,43−45] The only theoretical investigation of the hydroxyl radical in the *bulk* of 250 water molecules we are aware about has been performed[34] by classical Monte Carlo

† Stockholm University.
‡ Bogolyubov Institute for Theoretical Physics of the National Academy of Sciences of Ukraine.
* Corresponding author. E-mail: julia@physc.su.se.

10.1021/jp0461807 CCC: $30.25
Published on Web 12/07/2004

simulations with the interaction potentials derived from the cluster ab initio simulations.

In the present paper we report the results of the first to our knowledge ab initio type simulations of the hydroxyl radical solvated in the bulk water. For this purpose we employ Car−Parrinello[46] molecular dynamics technique that has been successfully used for investigation of the properties of liquid water,[47−53] its proper defects (hydronium and hydroxide ions),[54−56] and aqueous solutions of other ions[57−59] and molecules.[60,61]

2. Simulation Details

Our system consists of one hydroxyl and 31 H_2O molecules. The cubic simulation cell has the length 9.848634 Å. Periodic boundary conditions are applied. The resulting density of 1 g/cm^3 corresponds to the density of water at ambient conditions. The simulation temperature was 310 K.

Car−Parrinello[46] molecular dynamics simulations are performed with the help of CPMD[62] code. To account for a dangling bond at the hydroxyl radical,[36,40] the local spin density approximation (LSDA) functional theory is employed. The gradient corrected Becke−Lee−Yang−Parr (BLYP) exchange and correlation functional[63,64] is used since it has been shown to accurately reproduce the properties of aqueous systems.[47,48,57,65] The valence electronic wave functions are described in the plane wave basis with an energy cutoff of 75 Ry. The valence-core interactions are described by the norm-conserving Goedecker pseudopotentials. Two simulations runs have been carried out, with fictitious electron masses of 600 and 800 au. The fictitious electron kinetic energy is controlled by a chain of three Nose−Hoover thermostats[66−68] operating at characteristic frequency 6000 cm^{-1}. Such control is necessary in long (many ps) simulations to counter to leaking of energy from the ionic subsystem to the electronic degrees of freedom. The average fictitious kinetic energy is maintained at levels of 0.035 and 0.06 Ha in runs with electron masses 600 and 800 au correspondingly and remains stable during the whole simulation. The dynamics of atoms is also controlled by Nosé−Hoover thermostat operating at characteristic frequency 2000 cm^{-1}.

To start the simulations, a short classical molecular dynamics run for a system of 32 water molecules has been performed. After that, one of the hydrogen atoms was removed and the obtained atomic configuration was used as an input to CPMD run. The first 2 ps of CPMD dynamics are considered as equilibration time and discarded. We have performed two runs starting from different initial conditions, using the computer facilities at two supercomputer centers. One 41 ps production run has been performed using 32 CPUs of 2.2 GHz Linux cluster,[69] and for the second 30 ps production run 32 CPUs of 160 MHz SP2 supercomputer have been employed.[70] The time step was set to 0.1 fs. The only difference between the two runs was the fictitious electron mass, 600 au in the 41 ps run and 800 au for the second run. The results reported below are averaged over the two production runs, unless otherwise stated.

3. Results and Discussion

In what follows we denote the oxygen and the hydrogen atoms of the hydroxyl radical as O* and H*, respectively. Oxygens and hydrogens belonging to water molecules are denoted as O and H as usual.

3.1. Radial Distribution Functions. The radial distribution functions (RDF) obtained in our simulations are shown in Figure 1. In all cases, the bin width for RDF calculations was 0.05 Å.

Figure 1a represents the oxygen−hydrogen RDFs calculated for intrahydroxyl (O*−H*), hydroxyl−water (O*−H and O−H*), and water−water (O−H) distributions. Noteworthy, that the hydroxyl−water distribution functions generally follow the water−water O−H RDF. The position of the first intermolecular peak is 1.9 Å for all the three curves. However, both hydroxyl−water peaks are higher, and the O*−H peak is broader than the O−H one. As a result, the running hydrogen coordination number $n_{O^*H}(r)$ for hydroxyl oxygen atom is higher than $n_{OH}(r)$ for water oxygens, even if one takes into account the presence of H* in the system when calculating the hydrogen coordination number for water (see Table 1).

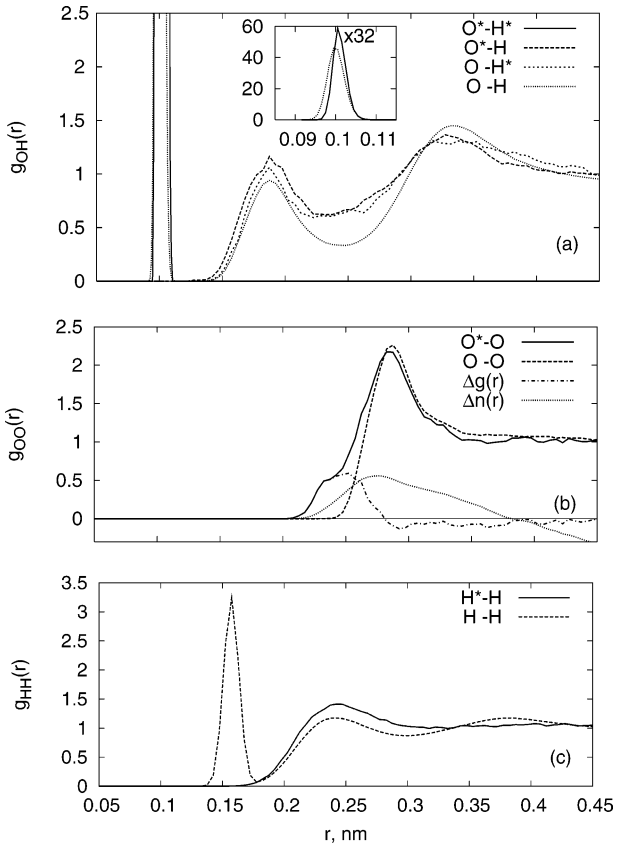

Figure 1. Oxygen−hydrogen (panel a) partial radial distribution functions for the hydroxyl (O*−H*, solid line), hydroxyl−water (O*−H, long-dashed line), water−hydroxyl (O−H*, short-dashed lines), and water−water (O−H, dotted line) distributions. The inset shows a detailed view of the first intramolecular peak with the hydroxyl radial distribution function having been reduced by a factor of 32. O−O and H−H radial distribution functions are shown in panels b and c with solid lines for hydroxyl−water and with dashed lines for water−water distributions. Difference $\Delta g(r)$ between O*−O and O−O RDFs is given by a dash−dotted line in the panel b. The dotted line represents the difference $\Delta n(r)$ between the running oxygen coordination numbers for the hydroxyl oxygen and for the water oxygen atoms.

The same is true for the case of the oxygen coordination number for hydrogen atoms ($n_{H^*O}(r) > n_{HO}(r)$). This means that the hydroxyl radical is more active both as a proton donor and as a hydrogen bond acceptor than the water molecule is, in difference with the results of classical Monte Carlo simulations[34] implying lower activity of the OH radical as a proton acceptor ($n_{O^*H}(r) = 1.2$ at $r = 2.3$ Å vs our value of 1.933).

The first minima of both $g_{O^*H}(r)$ and $g_{OH^*}(r)$ are less pronounced (0.62 and 0.59) than the water−water $g_{OH}(r)$ minimum (0.33) and are shifted to shorter distances (cf. Table 1). The second maxima of the hydroxyl partial RDFs are also shifted to the shorter distances and somewhat less pronounced than the water one. These features indicate that the first solvation shell of the hydroxyl radical is comparatively less structured.

TABLE 1: Running Coordination Numbers for Hydroxyl (O*H, O*O, and H*O) and Water (OH, OO, and HO)[a]

	r, nm	*n*(*r*)		*r*, nm	*n*(*r*)
O*H	0.225	1.802	H*O	0.225[m]	0.774
	0.235[m]	2.070		0.235	0.905
	0.245	2.367		0.245	1.050
	2.533	2.533		0.250	1.130
	0.450	24.70		0.450	12.54
OH	0.225	1.364 (1.389)	HO	0.225	0.682 (0.711)
	0.235	1.525 (1.554)		0.235	0.762 (0.795)
	0.245	1.684 (1.718)		0.245	0.842 (0.880)
	0.250[m]	1.768 (1.802)		0.250[m]	0.884 (0.925)
	0.450	23.69 (24.09)		0.450	11.84 (12.24)
O*O	0.240	0.185	OO	0.240	0.000 (0.006)
	0.340	5.149			
	0.365	6.434		0.340	4.713 (4.879)
	0.450	12.33		0.450	12.24 (12.64)

[a] Atoms from the same molecules are not taken into account. Numbers in parentheses are corrected for the presence of H* or O* in the vicinity of a water molecule. Positions of the RDFs minima are denoted with a superscript m.

The internal O*−H* peak is shifted to longer distances by 0.008 Å (Figure 1a, inset) compared to the length of the water covalent OH bond (1.006 against 0.998 Å), that agrees with the values 1.007 and 0.987 Å obtained for the clusters of six molecules by the density functional theory (DFT) calculations.[34]

The oxygen−oxygen RDF for hydroxyl−water distribution follows closely the water O−O RDF (see Figure 1b) starting from the maximum at 2.8 Å. At shorter distances, there is an excess of the probability to find an oxygen atom in the vicinity of O*. The excess distribution (dash−dotted line) spans a region between 2.1 and 2.8 Å with a maximum at 2.55 Å and probably corresponds to a hemibonded $H_2O{\cdot}OH$ complex with the O−O distance of 2.3 Å found in cluster simulations.[45]

The difference $\Delta n(r)$ between the running oxygen coordination numbers for O* and O is shown in Figure 1b with a dotted line. For the water oxygens, all the oxygen atoms (including O*) found within a certain distance from a central atom are taken into account. The difference has a maximum of $\Delta n_{max} = 0.559$ at $r = 2.8$ Å, where $g_{O*O}(r)$ and $g_{OO}(r)$ become equal. At longer distances, the O*−O RDF curve lies slightly lower than the water O−O RDF curve. As a result, $\Delta n(r)$ goes down to 0 at $r = 3.8$ Å and further to -0.31 at $r = 4.5$ Å (cf. the values of n_{O*O} and parenthetical n_{O*O} in Table 1).

The hydrogen−hydrogen (Figure 1c) distribution function for the hydroxyl is also quite close to the intermolecular part of the water H−H RDF. The only difference is a slightly higher first maximum at $r = 2.4$ Å (consistent with the higher number of hydrogen bonds accepted by O* and donated by H*). Another important feature is the absence of any minimum of $g_{H*H}(r)$ at $r \approx 3$ Å. Together with the absence of the first $g_{O*O}(r)$ minimum at $r \approx 3.5$ Å, this indicates a more diffuse first solvation shell than the one inherent to liquid water.

The obtained radial distribution functions turned out to be rather different from the results of the classical Monte Carlo simulations.[34] Apart from the inherent limitations of the classical potentials, the possible reason for this disagreement may be the fact that the interaction potentials of work[34] were derived from ab initio **cluster** simulations. However, the restricted size of the clusters (up to six water molecules) does not allow one to model a complete solvation shell. The tendency of the cluster calculations to give the maximum possible number of hydrogen bonds in the system leads to a displacement of the radical to a cluster edge. Therefore, the charge distribution in the OH obtained from the cluster simulations rather corresponds to the OH radical at the water surface than to the hydrated OH, and the reliability of the subsequent classical simulations becomes questionable.

Worth noting is also the absence of the minimum in the *water−water* O−O RDF (Figure 1b). Earlier ab initio simulations[47,49,50−53,65] as well as the results of the neutron scattering[71,72] and the X-ray diffraction experiments[73−75] for liquid water report a minimum of the oxygen−oxygen RDF at $r = 3.3$ Å. Also, the first maxima of O−O and O−H RDFs are lower that those observed in the earlier ab initio simulations of pure water. To clarify the situation, we have identified five water molecules closest to O* for every moment of time (5 is the value of the oxygen running coordination number for hydroxyl oxygen at $r = 3.4$ Å) and analyzed the partial radial distribution function for these five molecules. It has turned out that the O−O RDF between the nearest hydroxyl neighbors has a broad first maximum centered at $r = 3.5-3.7$ Å (not shown in Figure 1). Superimposed with the O−O distribution of the outer molecules, this maximum could be able to cancel out the minimum at 3.3 Å.

The different behavior of waters RDF observed in the present simulation cannot be however explained by only the molecules in the first hydration shell. Our analysis shows that the water structure is disturbed (though in a less degree) even outside the first solvation shell. The OH radical with its unpaired electron is clearly a stronger perturbation of the surrounding water structure than closed-shell ions. Analysis of electron density (see section below) shows that at least one water molecule bears an appreciable share of uncompensated spin density which affect interaction of this molecule with molecules in the second hydration shell. Additional factors which may contribute to the disappearance of the first minimum of O−O RDF is a slightly higher than ambient temperature in our simulation (310 K) and the small size of the simulation cell. In fact, our 9.8486 Å cubic cell does not allow to accommodate properly the second solvation shell of a water molecule (since the second minimum of water O−O RDF[51] is located at 5.5 Å) and to form the bulk water beside the hydroxyl radical. Therefore, most of the outer water molecules belong to the second solvation shell of the hydroxyl, which can be partially distorted by the finite size of the simulation cell.

To clarify this point, the more extensive simulations with a bigger system size should be done. In the rest of the present paper, we pay attention mostly to the properties of the first solvation shell.

3.2. Local Structure around the Hydroxyl. The considered so far radial distribution functions provide us with the basic structural information where angular and orientational dependencies are averaged out. To get a more detailed insight into the local hydration structure, we analyze the two- and three-dimensional distributions for the atoms located within the distance $r_{max} = 3.65$ Å from the hydroxyl oxygen. The chosen value of the maximum distance corresponds to the first (very shallow) minimum of $g_{O*O}(r)$.

First we consider the angle θ_{H*O*-X} (X is either O or H) between the hydroxyl axis and the direction from the O* to the X atom. Distributions $P(\theta_{H*O*-X}, r_{O*X})$ for the atoms belonging to water molecules are presented in Figure 2.

The distribution function $P(\theta, r)$ is normalized so as to integrate to the average number N of atoms found within the sphere of the radius r_{max}:

$$\int_0^{\pi}\int_0^{r_{max}} P(\theta, r) r^2 \, dr \, \sin\theta \, d\theta = N \qquad (1)$$

In our analysis, we divide the hydroxyl neighbors into two groups. Group I contains water molecules that are hydrogen

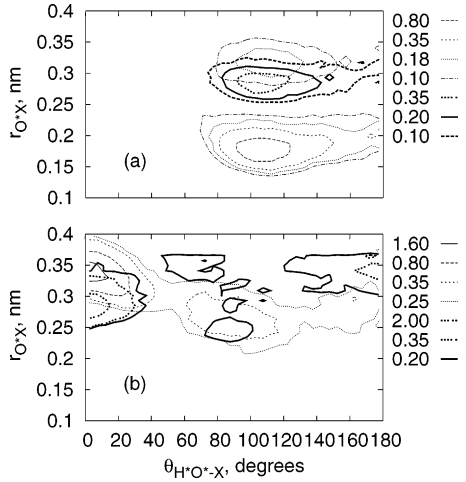

Figure 2. Contours of the two-dimensional distribution functions of the H*O*−X angle and of the O*−X distance calculated for the first solvation shell water molecules hydrogen bonded to the hydroxyl oxygen O* (panel a), and not bonded to it (panel b). X denotes O (thick lines) or H (thin lines).

bonded (H-bonded) to the hydroxyl oxygen. Molecules that are not H-bonded to O* fall into group II. For definition of a hydrogen bond we used a geometrical criterion: a water molecule is considered to be hydrogen bonded, if the O*−H distance is less than 2.45 Å and the O*−OH angle is less than 30°. The average number of molecules in group I is calculated to be 1.688, that is significantly less (by 0.679) than the running hydrogen coordination number $n_{O^*H}(r)$ of the hydroxyl oxygen at $r = 2.45$ Å. The $\theta_{H^*O^*-O}$ angle distribution for the molecules from group I (Figure 2a) is centered at ∼105° and resembles the corresponding angle distributions[55] for the water molecules in the solvation shell of the hydroxide ion OH^- (i.e., the whole distribution is shifted toward less angles as compared to the case of the bulk water). At the same time the distribution of the O*−O distance for the group I molecules is centered at 2.8 Å like the O−O distance in pure water, being different from the value of 2.65 Å for the hydroxide ion solvation shell.[55] Inspection of the O*−H distances and the O*−HO angles for the hydrogen bonds accepted by the hydroxyl radical shows close resemblance to the properties of the hydrogen bonds in liquid water and is not illustrated here. The distribution $P(\theta_{H^*O^*-H}, r_{O^*H})$ for the hydrogen atoms is shown in Figure 2a. The hydrogens participating in the hydrogen bonds with O* follow the pattern formed by the oxygens. The outer hydrogens have a slight tendency to decline toward the bigger $\theta_{H^*O^*-H}$ values.

The two-dimensional distributions for the molecules from group II are represented in Figure 2b. The distribution of the oxygen atoms shows clearly the presence of four different subgroups. Group IIa ($\theta_{H^*O^*-O} < 40°$ and 2.5 Å $< r_{O^*O} <$ 3.5 Å) consists mostly of the molecules accepting a hydrogen bond from H*. The rest of the group II molecules are not H-bonded to the hydroxyl radical in any way.

Group IIb contains water molecules with the oxygen atom very close to O* (2.1 Å $< r_{O^*O} <$ 3.1 Å, 70° $< \theta_{H^*O^*-O} <$ 110°) and both hydrogen atoms directed outward. These molecules form the excess of O*−O radial distribution function at small distances (see Figure 1b). There exist however some discussions whether such hemibonded coordination with short O − O distance is an artifact of the density functional theory and particularly the BLYP functional. Studies of small radical clusters[45,76] have shown that the BLYP functional may overestimate the strength of hemibonded structures due to the lack

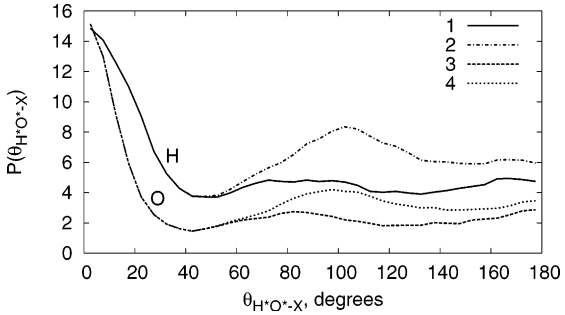

Figure 3. Distribution of the angles H*O*−H (1,2) and H*O*−O (3,4) for the first solvation shell molecules. The contribution of molecules not hydrogen bonded to O* is shown by curves 1 and 3, while adding the contribution from the hydrogen bonded water molecules results in the curves 2 and 4.

of Hartree−Fock exchange in the Becke's exhchange functional. Unfortunately, reference 45 gives insufficient structural information on the hemibonded $H_2O{\cdot}OH$ complex to relate it to our case. On the other hand, the dipole−dipole structures observed in the cluster calculations[34] employing a modified Perdew−Wang exchange functional clearly have the similar geometry, though the O*−O distance of about 2.8 Å and its tendency to increase with the cluster size observed in that work do not completely fit to our closely located molecules.

Group IIc, consisting of non-H-bonded molecules with $\theta_{H^*O^*-O} > 120°$, can be considered as a continuation of the H-bonded branch at larger H*O*−O angles, since these molecules have one of the hydrogen atoms directed to the hydroxyl oxygen. The hydrogen bonded molecules with the large H*O*−O angle and slightly longer O*−O distances have been also found in the solvation shell of the hydroxide ion.[55] The fourth (IId) group of non-H-bonded molecules at 40° $< \theta_{H^*O^*-O} <$ 90° and $r_{O^*O} > 3.2$ Å comprises the molecules that actually belong to the second solvation shell. The average number of water molecules in the group II(a−d) sums up to give 4.75.

The resulting distributions of the angles $\theta_{H^*O^*-X}$ obtained by the integration over the distances $r_{O^*X} < 3.65$ Å are shown in Figure 3.

The distribution function $P(\theta)$ is again normalized to the average number N of the atoms found within 3.65 Å distance from O*:

$$\int_0^{\pi} P(\theta) \sin\theta \, d\theta = N \qquad (2)$$

The distributions produced by the group II molecules (curves 1 and 3 in Figure 3) have the strong peaks at $\theta_{H^*O^*-X} < 40°$ formed by the molecules accepting the hydrogen bond from the H*. At larger angles they are quite smooth, the peaks due to groups IIb and IIc being relatively broad and poorly pronounced. The contributions from the group I water molecules show strong broad peaks centered at $\theta_{H^*O^*-X} \sim 105°$ that do not completely die out toward 180°.

The relative arrangement of the water molecules in the hydroxyl solvation shell is illustrated in Figure 4 by the distribution $P(\theta_{O-O^*-O}, r_{O^*O})$. The distribution is substantially diffuse (note the value of the lowest level). Its main maxima are located at the sphere of the radius of 2.8 Å (the maximum of O*−O RDF) at the O−O*−O angles of 70−100°, 160, and 180°. The additional maximum at $\theta_{O-O^*-O} \approx 50°$ and $r_{O^*O} \approx$ 3.5 Å clearly corresponds to the second solvation shell molecules.

There seems to be a slight preference to have four molecules in the lateral belt of the first solvation shell, which corresponds

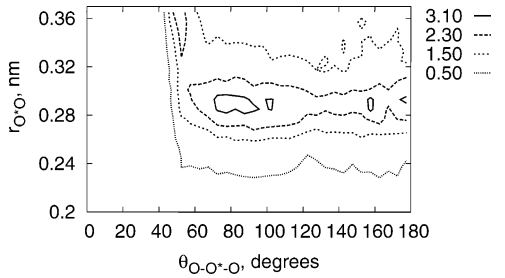

Figure 4. Contours of the two-dimensional distribution functions of the O−O*−O angle and of the O*−O distance for the first solvation shell.

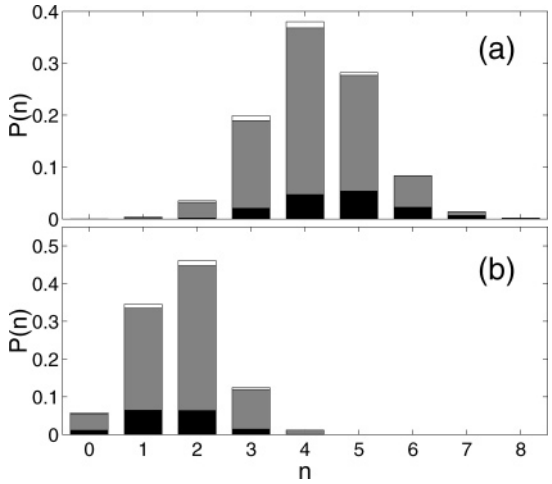

Figure 5. Number distribution of the first solvation shell molecules not accepting a hydrogen bond from H* (panel a) and the number distribution of the hydrogen bonds accepted by O* (panel b). The share of states without hydrogen bonding at H* is given by the filled area. The shaded area represents the states with the hydroxyl donating a hydrogen bond to a water molecule. The rest of the states have two water molecules in the group IIa.

to typical hydration structures observed for the OH^- ion.[54] This is confirmed by the number distribution of water molecules with $\theta_{H^*O^*-O} > 40°$ (Figure 5a). The distribution is calculated for $r_{O^*O} < 3.4$ Å to exclude the effect of the second solvation shell seen in Figures 2 and 4.

The average number of non-H*-bonded water molecules in the first solvation shell is 4.22. In the absence of the hydrogen bond at H* it increases to 4.63 as compared to the value of 4.16 in the presence of such bond. Absence of a hydrogen bond donated by the hydroxyl radical even decreases the number of accepted hydrogen bonds (down to 1.54 from the value of 1.72 expected in the presence of the H* bond, see Figure 5b). The average number of H*-bonded molecules (0.88) in the solvation shell together with 1.69 for the hydroxyl oxygen H-bonded ones sums up to the average of 2.56 water molecules hydrogen bonded to the hydroxyl radical. Taking into account 2.53 not-hydrogen-bonded molecules, the first solvation shell contains 5.09 water molecules. The distribution over the number of molecules in Figure 5 is rather broad, which manifests a generally loose structure of the first solvation shell.

Three-dimensional spatial distribution functions (SDF) for the water molecules in the vicinity of the hydroxyl radical are presented in Figures 6 and 7. All three-dimensional distributions have a solid maximum corresponding to a group IIa water molecule. The maximum always possess the axial symmetry implying that the orientation of the hydrogen bond accepted by this molecule and of the molecule itself are not correlated to other molecules in the solvation shell.

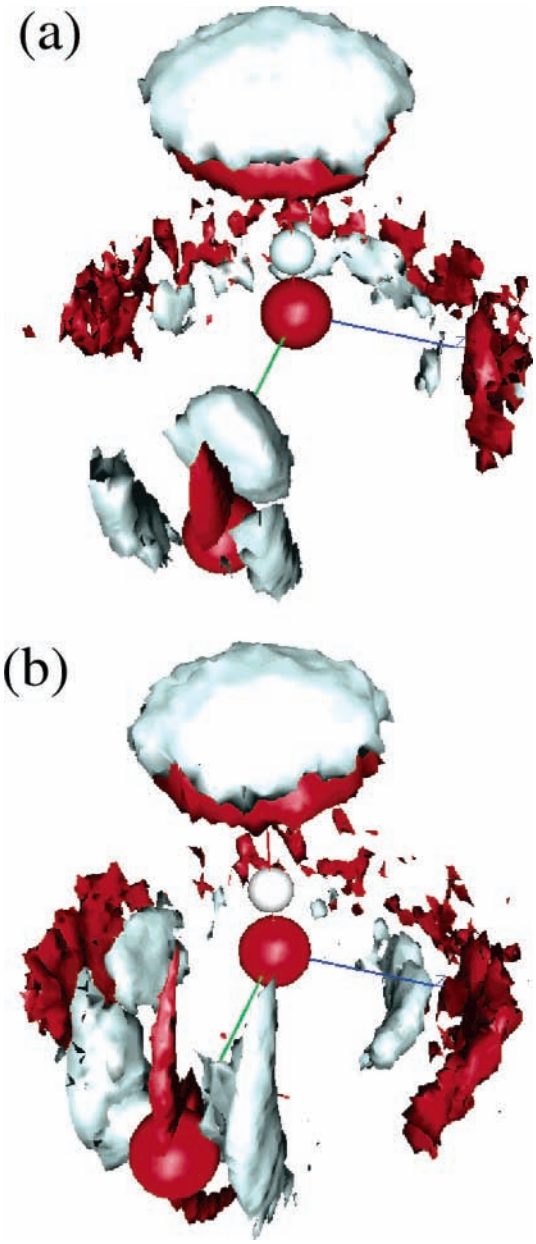

Figure 6. Isosurfaces of the spatial distributions with respect to the H*O*−O reference system shown in red (dark) for the oxygen atoms and in light gray for the hydrogen atoms. For panel a, the reference system is formed by the hydroxyl and an oxygen belonging to the group I water molecule, with SDF level is 50 for the reference water oxygen, 4.5 for other oxygen atoms, and 4.0 for hydrogen atoms. Panel b displays SDF for the group II reference waters with the SDF levels 35, 5.0, and 4.5, respectively.

Shown in Figure 6 are the distribution functions calculated in the reference system formed by the radical and a water oxygen belonging either to group I or to group II water molecules. The *x* axis is directed up along the hydroxyl, and the *z* axis (directed to the right) is perpendicular to the H*O*−O plane. Figure 6a represents the case of the reference water being hydrogen bonded to the hydroxyl oxygen. A wide hydrogen maximum at the line connecting the reference oxygens belongs to a water hydrogen forming the hydrogen bond. The other hydrogen atom gives rise to the two elongated blobs outside the water oxygen. The fact of elongation is due to the uncertainty of the oxygen position in the *xy* plane (shown as a salience in the upward direction), otherwise the O−H direction is not correlated with the hydroxyl axis.

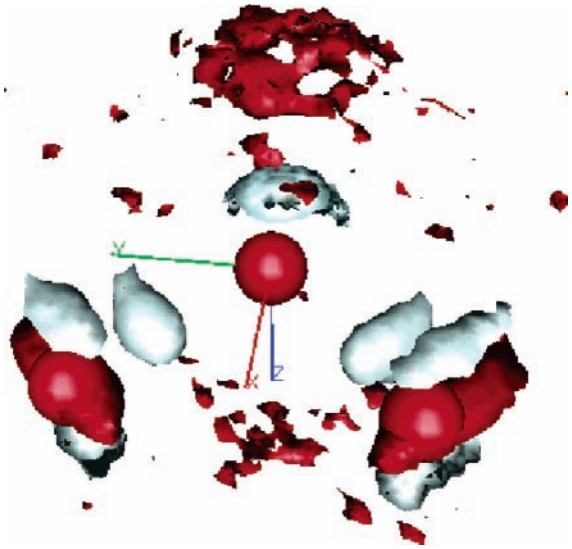

Figure 7. Isosurfaces of the spatial distributions with respect to O−O*−O reference system formed by O* and oxygens of two water molecules in the first hydration shell, with the H* atom directed up. The *x* axis is a bisector of the O−O*−O angle. Coloring is the same as in Figure 6. SDF level is 50 for the reference oxygens, 4.9 for other oxygens, 7.0 for water hydrogens, and 800 for H*.

An almost smooth distribution of both oxygen and hydrogen atoms in the lateral belt behind the hydroxyl implies weak correlation between the positions of group I water molecules. A slightly higher probability to find an oxygen atom at the belt edges at the intersection with the *z* axis implies higher correlation between group I and group IIb−d molecules. The correlation becomes more clear from the distributions calculated for the reference system based on the water molecules not H-bonded to the hydroxyl (Figure 6b). Both hydrogen and oxygen distributions have pronounced side lateral maxima, implying the presence of H-bonded group I water molecules at the angle of ∼90° to the *y* axis.

The spatial distribution functions of the reference water itself (note the long upward and downward protuberances of the oxygen isosurface) are strongly influenced by a wide range of the O−O*−H* angle fluctuations. The hydrogen blobs are much wider than for H-bonded reference molecules, and are located at the same distance from O* as the oxygen maximum is. The existence of the group IIb water molecules gives rise to the cusp in the direction to the hydroxyl oxygen (along the *y* axis) present in the reference oxygen SDF isosurface.

Low correlation between the positions of water molecules in the first hydration shell of the hydroxyl becomes more apparent through the spatial distribution functions calculated for the reference system based on the hydroxyl oxygen and the oxygen atoms of two water molecules shown in Figure 7. The flat features around the reference oxygens reflect the broad distribution of θ_{O-O^*-O} seen in Figure 4. The pronounced hydrogen maxima belong to the reference molecules solely (three maxima for each of the two waters, and one maximum for the H*). As to the oxygens distribution, there is only a clear oxygen maximum at the top of the figure (above the hydroxyl hydrogen) due to the group IIa molecules and a weaker maximum at the bottom corresponding to the group IIc molecules. Correspondingly, positions of other water molecules are poorly defined in this reference frame.

Remarkably, we have not been able to refine the above three-dimensional distributions by considering separately configurations with different number of water molecules in the hydration shell or with different number of hydrogen bonds accepted by the hydroxyl, as it was done for the OH^- case.[55]

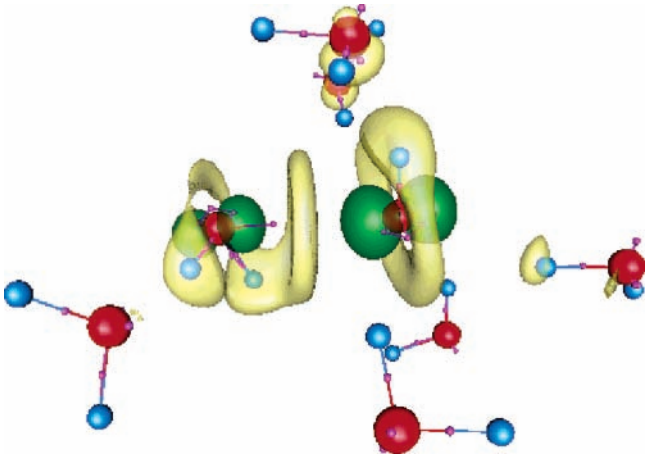

Figure 8. Isosurfaces of the spin density at the levels of −0.03 (dark green) and +0.0004 (yellow). Oxygen atoms are red, hydrogen atoms are light blue, and the centers of the Wannier functions are small pink balls.

3.3. Electron Density. The electronic properties of the hydrated hydroxyl radical are illustrated in Figure 8 with a snapshot from the molecular dynamics trajectory. Since the total spin of the system is $-1/2$, most of the *negative* spin density is located at the hydroxyl oxygen. Besides, there is usually a water molecule that carries an appreciable share of the negative spin. In the presence of a group IIb water molecule in the solvation shell it becomes a "chosen" one as in Figure 8 (the molecule to the left). Otherwise the excessive negative spin is shared with a group I water molecule.

Shown in Figure 8 is also an isosurface (yellow) of the low *positive* spin density that has a characteristic ring profile with a bulb at H*. The positive spin density is also observed at the "chosen" water molecule. For the case of hydrogen bonded molecules, it appears at the donated hydrogen. For the group IIb molecules the positive spin density is located near the center of the Wannier function elongated toward O*. This picture supports the identity of the group IIb molecules with the hemibonded water molecule from the $H_2O{\cdot}OH$ complex resulting from the three-electron bond between a lone pair of H_2O and the unpaired electron of the hydroxyl radical.[45]

3.4. Hydrogen Transfer. During 72 ps of CPMD simulations, one act of the hydrogen atom transfer from a water molecule to the hydroxyl radical has been observed. Before the act of transfer, the hydroxyl molecule accepts three hydrogen bonds and has almost ideal tetrahedral configuration (the left part of Figure 9). At the same time, the closest water molecule (to the right from hydroxyl in Figure 9) donates two hydrogen bonds (one of them to the hydroxyl) and does not accept any. Then a hydrogen donor (another water molecule) comes close to that water. A hydrogen bond between the two waters is formed and the first water molecule is pushed toward the hydroxyl. A covalent bond between the H-bond donating water hydrogen and the hydroxyl oxygen is formed, while the covalent bonds of the first water become stretched forming a H_3O_2 complex. This complex breaks down after 2 fs with the formation of a new hydroxyl radical and a water molecule in the tetrahedral configuration.

Figure 9 shows the compound molecule in the middle of the hydrogen transfer process. The hydrogen moves to the left, and the uncompensated negative spin density is transferred to the right.

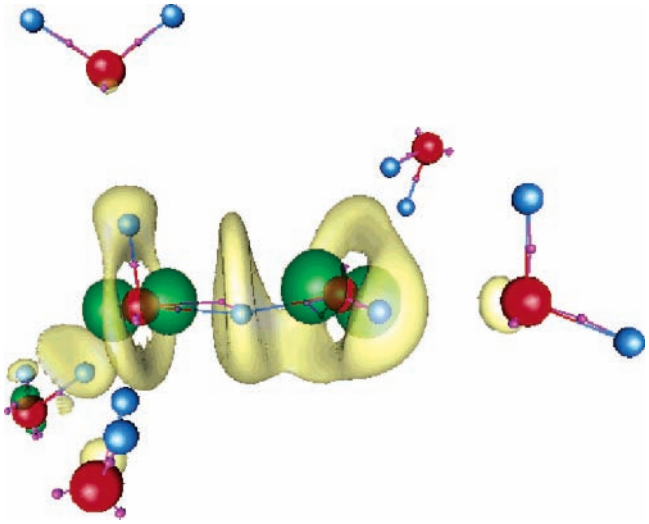

Figure 9. H_3O_2 complex in the process of the hydrogen transfer. Spin density levels and the coloring are the same as in Figure 8.

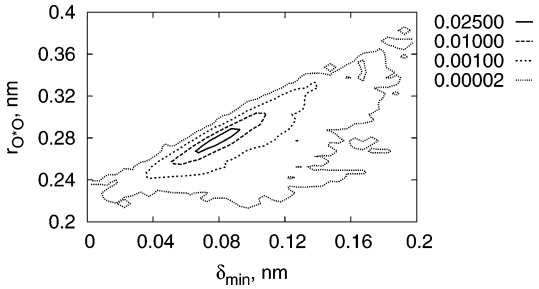

Figure 10. Contours of the two-dimensional distribution of δ_{min} and the O*−O distance for the first solvation shell water molecules.

The path for the hydrogen transfer is better seen in terms of the parameter δ_{min},[77] that is the shortest value of the asymmetric stretch coordinate

$$\delta = r_{O^*H} - r_{OH} \tag{3}$$

among the solvating water molecules. Configurations close to the hydrogen transfer should correspond to $\delta_{min} \approx 0$. The distribution of δ_{min} and r_{O^*O} for our system is plotted in Figure 10. While carrying no statistical significance, the leftmost part of Figure 10 clearly shows the path of one occurred hydrogen transfer to the hydroxyl radical. The transfer takes place at the O*−O distance of 2.4 Å and incorporates preparatory elongation of the water O−H covalent bond.

The central part of Figure 10 represents more statistically significant information on the strength of the hydrogen bonds accepted by the hydroxyl radical. Their relative weakness results in the maximum of the two-dimensional distribution at $\delta_{min} =$ 0.8 Å, while the corresponding maximum for the hydroxide ion solvation shell[55] is shifted to 0.5 Å.

The low statistics (one event in 72 ps) of the observed hydrogen transfers does not allow evaluation of the characteristic time of this event. Undoubtedly, however, is that for a hydroxyl radical this is much more rare event than for hydroxide or hydronium ions, for which the characteristic time of the hydrogen transfer is just a few picoseconds.[54] Due to this reason, the hydrogen hopping mechanism does not contribute much to the diffusion of OH radical. This is confirmed by the fact that the self-diffusion coefficient of OH radical in water (2.8, $\cdot 10^{-5}$ cm^2/s)[78] is just slightly higher than that of water molecules (2.3 $\times 10^{-5}$ cm^2/s) and much slower than diffusion coefficients of

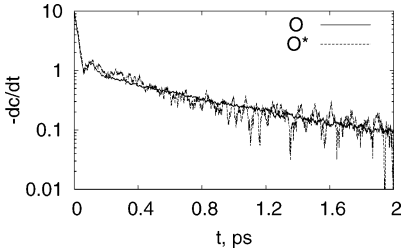

Figure 11. Reactive flux hydrogen bond correlation function for the water molecules (solid line) and for the hydroxyl oxygen (dashed line).

the aqueous ions (5×10^{-5} cm^2/s for OH^- and 9×10^{-5} cm^2/s for H^+).

3.5. Lifetime of Hydroxyl Hydrogen Bonds. An important characteristics of the hydrogen bonding in the system is the lifetime of a hydrogen bond t_{HB}. It can be determined as the time integral of the correlation function[79]

$$c(t) = \langle h(0)h(t)\rangle/\langle h\rangle \tag{4}$$

where $h(t)$ is a hydrogen bond population operator. For a given oxygen−hydrogen pair, h is equal to unity in the presence of the hydrogen bond, and is zero otherwise. If the number of hydrogen atoms in the system is N_H, the average number of hydrogen bonds accepted by a water molecule is $(N_H - 2)$-$\langle h\rangle_{O,H}$(= 1.441), where $\langle h\rangle_{O,H}$ denotes h averaged over all hydrogens, water oxygens, and time. The corresponding number of hydrogen bonds for the hydroxyl is and $(N_H - 1)\langle h\rangle$ (= 1.688), where the average $\langle h\rangle_{O^*,H}$ is taken over the pairs formed by O* and the water hydrogens.

The reactive flux hydrogen bond correlation function[79] $k(t) = -\mathrm{d}c/\mathrm{d}t$ characterizes the rate of relaxation of the hydrogen bonded system to the equilibrium and is plotted in Figure 11. The fast relaxation rate during the first 0.1 ps is usually attributed to hydrogen librations, and an additional peak at 0.1−0.2 ps is ascribed to interoxygen vibrations. Beyond this time scale, $k(t)$ decays monotonically for water (see solid line), but there is some additional hydrogen bond breaking activity for the hydroxyl at 0.2−0.4 ps. As a result, the lifetime of a hydrogen bond accepted by O* is 0.67 ps, which is considerably less than the 0.87 ps lifetime for water.

3.6. Time Correlation Functions and Vibrational Spectra. The dynamics of the atomic species is characterized by the velocity autocorrelation functions and their power spectra. To reduce the uncertainties due to the modest sampling for the correlation functions and to smooth out the Fourier spectra, we analyze the velocity autocorrelation functions by segments of the width $T = 1024$ fs. Segments are overlapped by half of their length. The Welch window[80]

$$W(t) = 1 - (2t/T - 1)^2 \tag{5}$$

is used to prevent the leakage from one frequency to another.

The resulting velocity autocorrelation power spectra calculated separately for the atomic species from the hydroxyl and from the water molecules are shown in Figure 12. The OH stretch for the hydroxyl radical shifts to lower frequencies by about 50 cm^{-1} as compared to water. This agrees with the longer O−H distance for the hydroxyl radical and with the results of the cluster simulations[34] that give 3105 cm^{-1} for the hydroxyl and 3355 cm^{-1} for water, both frequencies decreasing with the cluster size. The libration band of H* is slightly shifted to larger wavenumbers in agreement with the shift observed for the hydroxide ion.[55] The low-frequency (∼50 cm^{-1}) maximum of

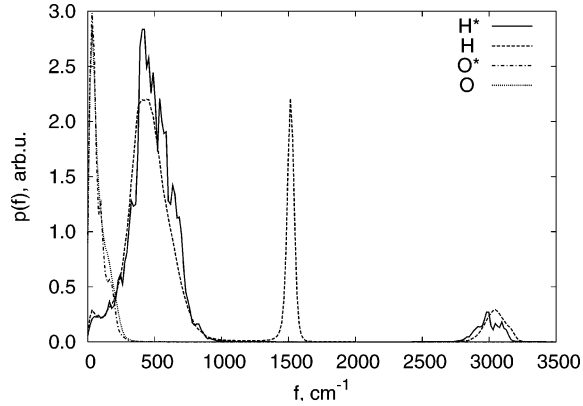

Figure 12. Velocity autocorrelation power spectra for the hydroxyl (H*) and water (H) hydrogens, as well as for the corresponding oxygen atoms (O* and O).

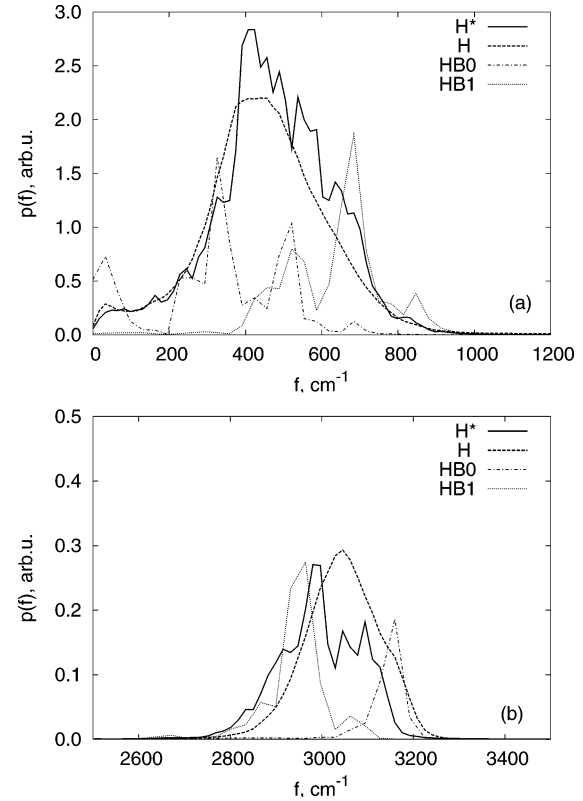

Figure 13. Detailed view of the libration (panel a) and the stretch (panel b) parts of the hydrogen velocity autocorrelation power spectra for H* and H. The partial spectra of the hydroxyl hydrogen participating (HB1) and not participating (HB0) in a hydrogen bond are also shown.

the hydrogen spectra corresponds to intermolecular motions, as is clearly seen from the oxygen spectra.

To clarify the structure of the H* spectrum, we extract from the simulation trajectory a few time intervals with the hydroxyl hydrogen being constantly hydrogen bonded to a water molecule, and a few intervals with a non-H-bonded H*. The velocity autocorrelation power spectra for H-bonded/non-H-bonded hydroxyl hydrogen are plotted in Figure 13. Because of a poor sampling, these spectra are calculated with the window (5) of the width $T = 512$ fs. It appears that the OH stretch frequency of non-H-bonded H* is shifted to larger wavenumbers by ~250 cm^{-1}. Since the hydrogen atom of the hydroxyl radical is preferably hydrogen bonded, the higher frequency peak is not pronounced in its spectrum. However, for the case of the not H-bonded OH^-, such peak gives a significant contribution to the spectrum.[55]

The blue shift of the H* libration band is also partly explained by the H-bonded states of H* (cf. the peak at ~700 cm^{-1} in Figure 13a). Since the non-H-bonded states are not statistically significant, the main maximum between 400 and 600 cm^{-1} is formed in the processes of breaking/creation of hydrogen bonds. This is in accord with ~0.07 ps time scale of the hydrogen bonding fast relaxation rate seen in Figure 11.

4. Conclusions

The results of Car−Parrinello molecular dynamics simulations of the hydroxyl radical in liquid water provide detailed information on the structural and dynamical properties of the OH aqueous environment. Computed radial and spatial distribution functions suggest a rather diffuse and poorly structured solvation shell of the OH with variety of configurations differing by the number of molecules in the shell and the hydrogen bonds between them. One of typically observed structures resembles a structure observed for OH^- ion[54] with one water molecule accepting hydrogen bond from H* of the hydroxyl and four water molecules in the perpendicular plane. However, in the case of the radical, only two of such waters donate hydrogens to the radical oxygen, other being not hydrogen bound (the group IIb waters). Apart from this structure, other configurations with four or six water molecules in the solvation shell or with other types of hydrogen bonding are often observed.

The existence of the group IIb water molecules is in fact a delicate question. They seem to correspond to a hemibonded H_3O_2 structure with a relatively short O- -O distance, that has been shown to appear in small clusters due to the lack of Hartree−Fock exchange in the Becke's exchange functional.[45] On the other hand, the dipole−dipole OH−H_2O complexes (but with larger O- -O distance) have been reported also for the small clusters modeled with a modified Perdew−Wang exchange functional.[34] To clarify this point, the simulations of the OH radical in liquid water with an exchange functional other than Becke's one are desirable.

Another open question is the structure of the second solvation shell of the OH radical. Since the present 10 Å simulation cell does not allow one to accommodate the second shell, some additional new simulations with a larger system size are needed.

Our simulations have shown that the proton exchange between hydroxyl radical and surrounding waters is a much more rare event than the hydrogen transfer between OH^- ion and water. This fact is related to the experimentally observed slower diffusion of OH radical comparing to the OH^- ion. Note however that the present simulations do not take into account the nuclear quantum effects on the dynamics of hydrogen atoms. These effects have been shown to be significant for the behavior of light nuclei.[53] While their computation is quite computationally expensive, the nuclear quantum effects are expected to be widely simulated in the nearest future.

Acknowledgment. We thank the National Supercomputer Center (NSC in Linköping, Sweden) and the Center for Parallel Computers (PDC at the Royal Institute of Technology in Stockholm) for granting computer facilities. The work was supported by the Swedish Research Council (Vetenskapsrådet).

References and Notes

(1) Halliwell, B.; Gutteridge, J. H. C. *Free radicals in Biology and Medicine;* Oxford University Press: Oxford, England 1989.

(2) Spinks, J. W. T.; Woods, R. J. *An introduction to radiation chemistry*; 3rd ed.; Wiley: New York, 1990.

(3) Kopenol, W. H. *Free Radical Biol. Med.* **1991**, *10*, 85.

(4) Stadtman, E. R. *Annu. Rev. Biochem.* **1993**, *62*, 797−821.

(5) Stumm, W.; Morgan, J. J. *Aquatic chemistry;* Wiley: New York, 1996.
(6) Aydogan, B.; Marshall, D. T.; Swarts, S. G.; Turner, J. E.; Boone, A. J.; Richards, N. G.; Bolch, W. E. *Radiat. Res.* **2002**, *157*, 38−44.
(7) Linert, W.; Jameson, G. N. L. *J. Inorg. Biochem.* **2000**, *79*, 319−326.
(8) Ren, J.-G.; Xia, H.-L.; Just, T.; Dai, Y.-R. *FEBS Lett.* **2001**, *488*, 123−132.
(9) Jay-Gerin, J.-P.; Ferradini, C. *Chem. Phys. Lett.* **2000**, *317*, 388−391.
(10) Tripathi, G. N. R.; Sun, Q. *J. Phys. Chem. A* **1999**, *103*, 9055−9060.
(11) Čík, G.; Šeršen, F.; Bumbálová, A. *Microporous Mesoporous Mater.* **2000**, *46*, 81−86.
(12) Chaychian, M.; Al-Sheikhly, M.; Silverman, J.; McLaughlin, W. L. *Radiat. Phys. Chem.* **1998**, *53*, 145−150.
(13) Acero, J. L.; Stemmler, K.; Gunten, U. *Environ. Sci. Technol.* **2000**, *34*, 591−597.
(14) Gårdfeldt, K.; Sommar, J.; Strömberg, D.; Feng, X. *Atmos. Environ.* **2001**, *5*, 3039−3047.
(15) Chameides, W. L.; Davis, D. D. *J. Geophys. Res.* **1982**, *87*, 4863.
(16) Chameides, W. L. *J. Geophys. Res.* **1984**, *89*, 4739.
(17) Staikova, M.; Donaldson, D. J. *Phys. Chem. Earth (C)* **2001**, *26*, 473−478.
(18) Stemmler, K.; von Gunten, U. *Atmos. Environ.* **2000**, *34*, 4241−4252.
(19) Stemmler, K.; von Gunten, U. *Atmos. Environ.* **2000**, *34*, 4253−4264.
(20) Chandra, A. K.; Uchimaru, T. *J. Phys. Chem. A* **2000**, *104*, 8535−8539.
(21) Upadhyaya, H. P.; Kumar, A.; Naik, P. D.; Sapre, A. V.; Mittal, J. P. *Chem. Phys. Lett.* **2001**, *349*, 279−285.
(22) Lien, P.-Y.; You, R.-M.; Hu, W.-P. *J. Phys. Chem. A* **2001**, *105*, 2391−2400.
(23) Smith, I. W. M.; Ravishankara, A. R. *J. Phys. Chem. A* **2002**, *106*, 4798−4807.
(24) Hobza, P.; ZahradnÂ×c1k, R. *J. Theor. Biol.* **1977**, *66*, 461−474.
(25) Schwarz, H. A.; Dodson, R. W. *J. Phys. Chem.* **1984**, *88*, 3643−3647.
(26) LaVere, T.; Becker, D.; Sevilla, M. D. *Radiat. Res.* **1996**, *145*, 673−680.
(27) Cermenati, L.; Pichat, P.; Guillard, C.; Albini, A. *J. Phys. Chem. B* **1997**, *101*, 2650−2658.
(28) Mohan, H.; Mittal, J. P. *Chem. Phys. Lett.* **2002**, *364*, 599−607.
(29) Kim, K. S.; Kim, H. S.; Jang, J. H.; Kim, H. S.; Mhin, B.-J.; Xie, Y.; Schaefer, H. F. *J. Chem. Phys.* **1991**, *94*, 2057−2062.
(30) Xie, Y.; Schaefer, H. F. *J. Chem. Phys.* **1993**, *98*, 8829−8834.
(31) Wang, B.; Hou, H.; Gu, Y. *Chem. Phys. Lett.* **1999**, *303*, 96−100.
(32) Zhou, Z.; Qu, Y.; Fu, A.; Du, B.; He, F.; Gao, H. *Int. J. Quantum Chem.* **2002**, *89*, 550−558.
(33) Cooper, P. D.; Kjaergaard, H. G.; Langford, V. S.; McKinley, A. J.; Quickenden, T. I.; Schofield, D. P. *J. Am. Chem. Soc.* **2003**, *125*, 6048−6049.
(34) Cabral do Couto, P.; Guedes, R. C.; Costa Cabral, B. J.; Martinho Simes, J. A. *J. Chem. Phys.* **2003**, *119*, 7344−7355.
(35) Wang, B.; Hou, H.; Gu, Y. *Chem. Phys. Lett.* **1999**, *309*, 274−278.
(36) Frank, I.; Parrinello, M.; Klamt, A. *J. Phys. Chem. A* **1998**, *102*, 3614−3617.
(37) Ricca, A.; Charles, W. Bauschlicher, J. *Chem. Phys. Lett.* **2000**, *328*, 396−402.
(38) Lundqvist, M. J.; Eriksson, L. A. *J. Phys. Chem. B* **2000**, *104*, 848−855.
(39) Wang, L.; Zhang, J. *J. Mol. Struct. (THEOCHEM)* **2001**, *543*, 167−175.
(40) Mundy, C.; Colvin, M.; Quong, A. *J. Phys. Chem. A* **2002**, *106*, 10063−10071.
(41) Suh, M.; Bagus, P. S.; Pak, S.; Rosynek, M. P.; Lunsford, J. H. *J. Phys. Chem. B* **2000**, *104*, 2736−2742.
(42) Cremer, D.; Kraka, E.; Sosa, C. *Chem. Phys. Lett.* **2001**, *337*, 199−208.
(43) Coe, J. V.; Earhart, A. D.; Cohenand, M. H.; Hoffman, G. J.; Sarkas, H. W.; Bowen, K. H. *J. Chem. Phys.* **1997**, *107*, 6023.
(44) Novakovskaya, Y. V.; Stepanov, N. F. *J. Phys. Chem. A* **1999**, *103*, 3285−3288.
(45) Hamad, S.; Lago, S.; Mejas, J. A. *J. Phys. Chem. A* **2002**, *106*, 9104−9113.
(46) Car, R.; Parrinello, M. *Phys. Rev. Lett.* **1985**, *55*, 2471−2474.
(47) Sprik, M.; Hutter, J.; Parrinello, M. *J. Chem. Phys.* **1996**, *105*, 1142−1152.
(48) Silvestrelli, P.; Bernasconi, M.; Parrinello, M. *Chem. Phys. Lett.* **1997**, *277*, 478−482.
(49) Silvestrelli, P.; Parrinello, M. *J. Chem. Phys.* **1999**, *111*, 3572−3580.
(50) Izvekov, S.; Voth, G. *J. Chem. Phys.* **2002**, *116*, 10372−10376.
(51) Head-Gordon, T.; Hura, G. *Chem. Rev.* **2002**, *102*, 2651−2670.
(52) Hura, G.; Russo, D.; Glaeser, R. M.; Head-Gordon, T.; Krack, M.; Parrinello, M. *Phys. Chem. Chem. Phys.* **2003**, *5*, 1981−1991.
(53) Chen, B.; Ivanov, I.; Klein, M.; Parrinello, M. *Phys. Rev. Lett.* **2003**, *91*, 215503.
(54) Tuckerman, M.; Laasonen, K.; Sprik, M.; Parrinello, M. *J. Chem. Phys.* **1995**, *103*, 150−161.
(55) Chen, B.; Ivanov, I.; Park, J.; Parrinello, M.; Klein, M. *J. Phys. Chem. B* **2002**, *106*, 12006−12016.
(56) Tuckerman, M. E.; Marx, D.; Parrinello, M. *Nature (London)* **2002**, *417*, 925−929.
(57) Ramaniah, L.; Bernasconi, M.; Parrinello, M. *J. Chem. Phys.* **1999**, *111*, 1587−1591.
(58) Lyubartsev, A. P.; Laasonen, K.; Laaksonen, A. *J. Chem. Phys.* **2001**, *114*, 3120−3126.
(59) Heuft, J. M.; Meijer, E. J. *J. Chem. Phys.* **2003**, *119*, 11788−11791.
(60) Sillanpää, A.; Päivärinta, J.; Hotokka, M.; Rosenholm, J.; Laasonen, K. *J. Phys. Chem. A* **2001**, *105*, 10111−10122.
(61) Chen, B.; Park, J.; Ivanov, I.; Tabacchini, G.; Klein, M.; Parrinello, M. *J. Am. Chem. Soc.* **2002**, *124*, 8534−8535.
(62) Hutter, J.; et al. CPMD version 3.7.2. Copyright IBM Corp 1990−2004, Copyright MPI für Festkörperforschung Stuttgart, Stuttgart, Germany, 1997−2001.
(63) Becke, A. *Phys. Rev. A* **1988**, *38*, 3098−3100.
(64) Lee, C.; Yang, W.; Parr, R. *Phys. Rev. B* **1988**, *37*, 785−789.
(65) Kuo, I.-F. W.; Mundy, C. J.; McGrath, M. J.; Siepmann, J. I.; VandeVondele, J.; Klein, M. *J. Phys. Chem. B* **2004**, *108*, 12990−12998.
(66) Nosé, S. *Mol. Phys.* **1984**, *52*, 255−268.
(67) Hoover, W. *Phys. Rev. A* **1985**, *31*, 1695−1697.
(68) Martyna, G. J.; Klein, M. L.; Tuckerman, M. *J. Chem. Phys.* **1992**, *97*, 2635−2643.
(69) *Monolith.* Pentium Xeon 2.2 GHz Linux Cluster, National Supercomputer Center, Linköping, Sweden, http://www.nsc.liu.se.
(70) *Strindberg.* IBM SP P2SC 160 MHz supercomputer, Center for Parallel Computers, KTH−Royal Institute of Technology, Stockholm, Sweden, http://www.pdc.kth.se.
(71) Soper, A. K.; Bruni, F.; Ricci, M. A. *J. Chem. Phys.* **1997**, *106*, 247.
(72) Soper, A. K. *Chem. Phys.* **2000**, *258*, 121.
(73) Narten, A. H.; Levi, H. A. *J. Chem. Phys.* **1971**, *55*, 2263.
(74) Hura, G.; Sorenson, J. M.; Glaeser, R. M.; Head-Gordon, T. *J. Chem. Phys.* **2000**, *113*, 9140−9148.
(75) Sorenson, J. M.; Hura, G.; Glaeser, R. M.; Head-Gordon, T. *J. Chem. Phys.* **2000**, *113*, 9149−9161.
(76) Sodupe, M.; Bertran, J.; Rodriguez-Santiago, L.; Baerends, E. J. *J. Phys. Chem. A* **1999**, *103*, 166−170.
(77) Tuckerman, M. E.; Ungar, P. J.; von Rosenvinge, T.; Klein, M. L. *J. Phys. Chem.* **1996**, *100*, 12878.
(78) Schwarz, H. A. *J. Phys. Chem.* **1969**, *73*, 1928−1937.
(79) Luzar, A.; Chandler, D. *Phys. Rev. Lett.* **1996**, *76*, 928−931.
(80) Press, W. H.; Teukolsky, S. A.; Vetterling, W. T. *Numerical Recipes in C*, 2nd ed.; Cambridge University Press: Cambridge, England, 1993.